Journal of the Nigerian Mathematical Society
Vol. 40, Issue 3, pp. 161-181, 2021

SIGNIFICANCE OF SUCTION AND DUAL STRETCHING: COMPARATIVE ANALYSIS BETWEEN THE DYNAMICS OF WATER-BASED ALUMINA NANOPARTICLE AGGREGATION WITH WATER-BASED CUPRIC NANOPARTICLE AGGREGATION

K. K. ASOGWA AND I. L. ANIMASAUN[1]

Suction and dual-stretching are valuable tools for influencing not only heat transfer but also friction. However, nothing is known about the impact of nanoparticles' volume fraction and aggregation. This report focuses on the significance of suction and dual stretching on the dynamics of water-based alumina nanoparticle aggregation and water-based cupric nanoparticle aggregation using the Maxwell-Bruggeman model. The governing equation that models the transport phenomenon mentioned above is presented, non-dimensionalized, and parameterized. The numerical solutions of the set of equations that are unitless were obtained using the Matlab package - `bvp4c`. Increasing suction and dual stretching are a yardstick to decline local skin friction coefficients proportional to heat transfer rate but cause Nusselt number proportional to the heat transfer rate. The rate of decrease in the local skin friction coefficients proportional to the friction is maximum in the transport phenomenon of water conveying alumina nanoparticles. The temperature distribution across the transport phenomena is a decreasing property of (a) Prandtl number, (b) dual stretching, (c) fractal index, and (d) maximum volume fraction of nanoparticles. The reverse is the case of volume fraction as it boosts the temperature distribution. The velocity functions are decreasing properties of radii of aggregates and nanoparticles, volume fraction, and suction.

Keywords and phrases: Suction, Dual stretching, Water-Alumina Nanofluid, Water-Cupric Nanofluid.
2010 Mathematical Subject Classification: 14F35, 76A05, 30E25, 76E06, 80A20

1. BACKGROUND INFORMATION

Received by the editors April 30, 2021; Revised: July 10, 2021; Accepted: July 27, 2021
www.nigerianmathematicalsociety.org; Journal available online at https://ojs.ictp.it/jnms/
[1]Corresponding author

The increasing body of knowledge on the importance of suction and dual stretching has helped the experts and researchers understand its influence on heat transfer, friction, temperature distribution across a flowing fluid, and momentum. The control, growth, and formation of nanoparticles to form clusters either by particle transport mechanisms or interfacial chemical reactions are known as the aggregation of nanoparticles (NPs) in the base fluid. The nanoparticles do not exist as individual particles in the fluid medium but tend to aggregate together due to interparticle forces. Aggregation of tiny particles in the base fluid was described by Zhang [1] as a factor capable of changing the physicochemical properties, reactivity, transport, and biological interactions of nanoparticles. Aggregation of colloidal particles in the base fluid has occurred when (a) the physical processes bring particle surfaces in contact with each other, (b) there exists a short-range in thermodynamic interactions, and (c) particle-particle attachment occurs. Stability is one of the crucial factors responsible for the overall benefits and the heat transfer augmentation of the hybrid nanofluids since the presence of nanoparticles determines strong van der Waals forces, thus creating aggregates. According to Ali [2], some of the advantages of the single-step method of preparing hybrid nanofluid are (a) excellent stability, (b) nanofluid homogenization, and (c) no particle aggregation. The last point made in Ref. [2] is valid because interactions in the transport of nanoparticles, as in the case of nanofluid made up of a single-step method, may cause the nanoparticles to adhere to each other and eventually avoid nanofluid homogeneity. But, it is challenging to prepare a homogeneous nanofluid with proper stability without particle aggregation. More so, evaporation of the fluid is a factor causing the aggregation of nanoparticles. In a study on the thermal conductivity, electrical conductivity, viscosity, and refractive index of two non-aggregating (stable) nanofluids of $\gamma - Al_2O_3$ and SiO_2 and two aggregating (unstable) nanofluids of TiO_2 and α-Al_2O_3 by Angayarkanni and Philip [3] that the effect of aggregation in unstable nanofluids leads to a substantial modification of their viscosity and refractive index.

Homo-aggregation and hetero-aggregation are two types of aggregation. Homo-aggregation refers to the aggregation of two particles of the same kind, while hetero-aggregation refers to dissimilar particles' aggregation. Homoaggregation under controlled laboratory conditions produces aggregates of reasonably predictable fractal dimension, whereas hetero-aggregation typically forms natural

fractals, making aggregation states more difficult to describe and predict Keller *et al.* [4]. Smaller particles aggregate more readily than larger particles because aggregation lowers the free energy of the system. Besides, the smaller the particle, the higher the surface energy. Results obtained by Babakhani [5] show that incorporating aggregation into the transport model improves the predictiveness of current theoretical and empirical approaches to nanoparticles deposition in porous media. More so, disregarding the acceleration factor, aggregation enhances nanoparticles mobility at regions close to the injection point at a field scale. It causes their retention at greater distances by altering their diffusivities, secondary interaction-energy minima, and settling behavior. He *et al.* [6] included nanoparticle aggregation in the heat transfer analysis of titania nanofluid in a pipe and discovered that the viscosity increases with nanoparticle aggregation.

Comparison of ethylene glycol's dynamics conveying aggregated and non-aggregated titanium nanoparticles due to Marangoni convection (i.e. surface tension at the wall) as seen in Mackolil and Mahanthesh [7] along an inclined wall when Lorentz force, thermal radiation, space, and temperature-dependent heat sources are significant. The results show that increasing Lorentz force, angle of inclination, and volume fraction made the transport phenomenon's velocity decline. Still, the velocity without aggregation is higher than the velocity with aggregation. This is true because nanoparticles' presence determines strong van der Waals forces, thus creating nanoparticle aggregation, and nanoparticle surfaces are in contact with each other, thus forming a kind of block that reduces the distance cover per time. Also, at all the chosen Lorentz force and volume fraction levels, it is evident in the results that the temperature distribution in the dynamics of ethylene glycol conveying aggregated titanium nanoparticles is higher than that of non-aggregate of nanoparticles. This indicates that not only does aggregation enhances nanoparticle mobility Babakhani [5], but the associated particle-particle attachment causes additional internal heating. More so, Van der Waals forces are independent of temperature except for dipole-dipole interactions.

The wide importance of nanoparticles in engineering and technology has prompted researchers to continue exploring newer nanotechnology areas. Thermal conductivity can be enhanced by clusters from the aggregation of nanoparticles reported by Ravi Prasher [8] in colloidal nanofluids. As a model compound, Titania was used

to investigate the effects of surface potential on subsurface particle mobility in Katherine *et al.* [9]. It was pointed out that the nanoparticle interactions with each other and surfaces are controlled by pH, and hence, surface potential and aggregate size increase as pH increases. Theoretical and experimental research carried out by Kleinstreuer and Feng [10] on nanofluid thermal conductivity enhancement. Using Kreiger and Dougherty (K-D) model used by Gaganpreet and Srivastava [11] to study nanofluids' thermal conductivity and viscosity by assuming that the nanoparticles may aggregate on dispersion. The results obtained for thermal conductivity align with the experimental results when the impact of various types of clusters is considered. Viscosity increases with the increase in particle aggregate (r_a) and matches well for $r_a = 3r$ at low concentration. Ellahi *et al.* [12] proposed a new model to study the effects of Al_2O_3 nanoparticle aggregation on water base fluid over a porous wedge. Peddiesona and Chamkha [13] considered nanofluid aggregation modeling and reported that nanofluid thermal conductivity is enhanced by nanoparticle aggregation. An Iron metal (F_e) nanoparticle aggregates in a water-based fluid to form clusters was reported by Marin *et al.* [14] under the influence of an external applied magnetic field over a stretching cylinder. It is worth deducing from the results that the heat transfer rate improved by increasing the number of particles in the backbone, while the wall shear stress is improved by increasing the dead-end particles. Additional references on the topic under discussion can be easily fetched in the report by Chen *et al.* [15], Animasaun *et al.* [16], Nanja *et al.* [17], Aladdin *et al.* [18], Devi and Devi [19], and Nadeem *et al.* [20].

Sequel to the outline reviewed of the literature, it is essential to study the significance of suction and dual stretching on the dynamics of water-based alumina nanoparticle aggregation and water-based cupric nanoparticle aggregation using the Maxwell-Bruggeman model. The study was initiated to provide logical answers to the following research questions:

(1) In the case of dynamics of water-based alumina nanoparticle aggregation and water-based cupric nanoparticle aggregation, what are the effects of dual stretching and suction on the local skin friction coefficients and Nusselt number of both nanofluids flow?
(2) How do volume fraction, fractal index, the maximum volume fraction of nanoparticles, and radii of aggregates &

nanoparticles affect the dynamics of water-based alumina nanoparticle aggregation and water-based cupric nanoparticle aggregation?

2. RESEARCH METHODOLOGY

In this section, the adopted research methodology for the study design to provide answers to the aforementioned research questions are presented.

2.1 FORMULATION OF THE GOVERNING EQ.

The steady and three-dimensional flow of water-based alumina nanoparticles and water-based cupric nanoparticles was considered in a rectangular frame of x, y, and z reference; see Figure (1). The velocities of the horizontal surface in x-direction and y-direction (i.e. $u_w = ax$ and $v_w = by$) were induced by a dual linear stretching following the exploration and extension of the boundary layer used by Prandtl [21] and Sakiadis [22]. The governing equation for the mechanics is of the form.

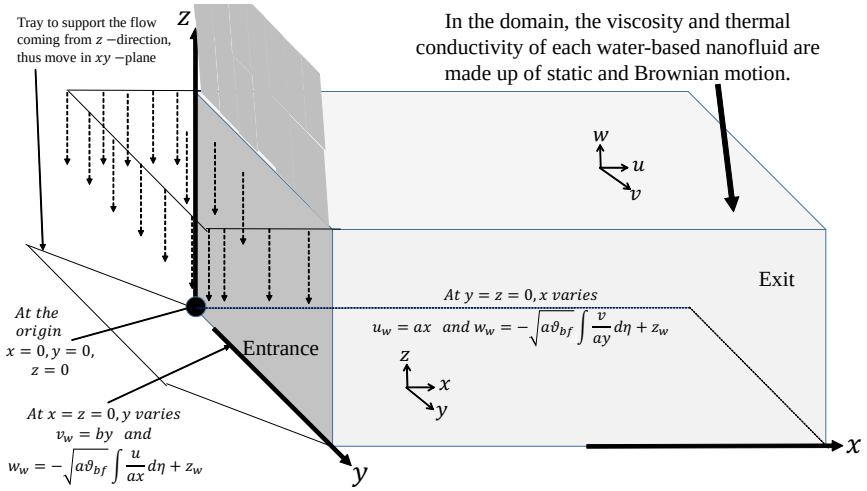

FIGURE 1. Physical Configuration in xyz-domain

$$\frac{\partial u}{\partial x} + \frac{\partial v}{\partial y} + \frac{\partial w}{\partial z} = 0, \tag{1}$$

$$u\frac{\partial u}{\partial x} + v\frac{\partial u}{\partial y} + w\frac{\partial u}{\partial z} = \frac{\mu_{nf}}{\rho_{nf}}\frac{\partial^2 u}{\partial z^2}, \tag{2}$$

$$u\frac{\partial v}{\partial x} + v\frac{\partial v}{\partial y} + w\frac{\partial v}{\partial z} = \frac{\mu_{nf}}{\rho_{nf}}\frac{\partial^2 v}{\partial z^2}, \tag{3}$$

$$u\frac{\partial T}{\partial x}+v\frac{\partial T}{\partial y}+w\frac{\partial T}{\partial z}=\frac{\kappa_{nf}}{(\rho Cp)_{nf}}\frac{\partial^2 T}{\partial z^2}. \tag{4}$$

Next is to present the boundary conditions. Along $x-$direction and at $y=0$, $z=0$ are

$$u=u_w(x)=ax,\ \ w=w_w\left(=-\sqrt{a\vartheta_{bf}}\int\frac{v}{ay}d\eta+z_w\right),\ \ \text{at}\ \ z=0,$$
$$\text{and}\ \ y=0. \tag{5}$$

$$u\to 0,\quad \text{as}\ \ z\to\infty\quad and\quad y=0. \tag{6}$$

Along $y-$direction and at $x=0$, $z=0$, boundary conditions are

$$v=v_w(x)=\frac{b^2y}{a},\ \ w=w_w\left(=-\sqrt{a\vartheta_{bf}}\int\frac{u}{ax}d\eta+z_w\right),\ \ \text{at}\ \ z=0,$$
$$\text{and}\ \ x=0 \tag{7}$$

$$v\to 0,\quad \text{as}\ \ z\to\infty\quad and\quad x=0. \tag{8}$$

Boundary conditions for Eq. (4) are

$$T=T_w,\quad \text{at}\ \ z=0\quad as\quad (x,y)\to\infty \tag{9}$$

$$T\to T_\infty,\quad \text{as}\ \ z\to\infty,\quad and\quad (x,y)\to\infty. \tag{10}$$

In addition to the data presented as Table 1, the effective thermo-

TABLE 1. Thermophysical properties of H_2O, Al_2O_3, and CuO used by Sheikholeslami *et al.* [23] and Mohammadein *et al.* [24]

	$\rho(kgm^{-3})$	$C_p(J/kgK)$	$\kappa(W/mK)$
H_2O	997.1	4179	0.613
Al_2O_3	3970	765	25
CuO	6500	540	18

physical properties are considered based on aggregation property are density of the nanofluid ρ_{nf}, the specific heat capacity of the nanofluid $(\rho Cp)_{nf}$, dynamic viscosity μ_{nf}, thermal conductivity κ_{nf}

$$\rho_{nf}=(1-\phi_a)\rho_{bf}+\phi_a\rho_{sp},\quad (\rho Cp)_{nf}=(1-\phi_a)(\rho Cp)_{bf}+\phi_a(\rho Cp)_{sp},$$
$$\mu_{nf}=\mu_{bf}\left(1-\frac{\phi_a}{\phi_m}\right)^{[\chi]\phi_m},\ \ \kappa_{nf}=\kappa_{bf}\left[\frac{\kappa_a+2\kappa_{bf}-2\phi_a(\kappa_{bf}-\kappa_a)}{\kappa_a+2\kappa_{bf}+\phi_a(\kappa_{bf}-\kappa_a)}\right]. \tag{11}$$

On introducing the following non-dimensional quantities

$$u = ax\frac{df}{d\eta}, \quad v = by\frac{dg}{d\eta}, \quad w = -\left(a\vartheta_{bf}\right)^{\frac{1}{2}}\left[f(\eta) + cg(\eta)\right], \quad c = \frac{b}{a},$$

$$\eta = z\left(\frac{a}{\vartheta_{bf}}\right)^{\frac{1}{2}}, \quad f_w = \frac{-z_w}{\sqrt{a\vartheta_{bf}}}, \quad \theta = \frac{T - T_\infty}{T_w - T_\infty}, \quad P_r = \frac{\vartheta_{bf}}{\alpha_{bf}}. \tag{12}$$

Where u, v, and w are velocity components in the x, y, and z directions, c is the stretching ratio, z_w is the dimensional suction parameter, f_w is the dimensionless suction velocity, (a and b) are the stretching rates, P_r is the Prandtl number, T is the dimensional fluid temperature. Substituting Eq. (20) and Eq. (12) into Eq. (1) - Eq. (10) to obtain

$$\frac{A_2}{A_1}\frac{d^3f}{d\eta^3} - \frac{df}{d\eta}\frac{df}{d\eta} + [f + cg]\frac{d^2f}{d\eta^2} = 0, \tag{13}$$

$$\frac{A_2}{A_1}\frac{d^3g}{d\eta^3} - c\frac{dg}{d\eta}\frac{dg}{d\eta} + [f + cg]\frac{d^2g}{d\eta^2} = 0, \tag{14}$$

$$\frac{A_4}{A_3}\frac{d^2\theta}{d\eta^2} + P_r f\frac{d\theta}{d\eta} + P_r cg\frac{d\theta}{d\eta} = 0. \tag{15}$$

Together with the set of boundary conditions

$$\frac{df}{d\eta} = 1, \quad f = f_w, \quad \frac{dg}{d\eta} = c, \quad g = \frac{f_w}{c}, \quad \theta = 1 \quad \text{at} \quad \eta = 0, \tag{16}$$

$$\frac{df}{d\eta} \to 0, \quad \frac{dg}{d\eta} \to 0, \quad \theta \to 0 \quad \text{as} \quad \eta \to \infty. \tag{17}$$

Where

$$A_1 = 1 - \phi_a + \phi_a\frac{\rho_{sp_1}}{\rho_{bf}}, \quad A_2 = \left(1 - \frac{\phi_a}{\phi_m}\right)^{[\chi]\phi_m},$$

$$A_3 = 1 - \phi_a + \phi_a\frac{(\rho C_p)_{sp}}{(\rho C_p)_{bf}}, \; A_4 = \left[\frac{\kappa_a + 2\kappa_{bf} - 2\phi_a(\kappa_{bf} - \kappa_a)}{\kappa_a + 2\kappa_{bf} + \phi_a(\kappa_{bf} - \kappa_a)}\right] \tag{18}$$

The aggregation model for thermal conductivity was derived by modifying the Maxwell model to obtain the Bruggeman model. The model was used because of its accuracy and the nanofluids' inherent aggregation property. Following Mackolil and Mahanthesh [7], the aggregate thermal conductivity modeled is of the form

$$\frac{\kappa_a}{\kappa_{bf}} = \frac{1}{4}\left[(3\phi_{in} - 1)\frac{\kappa_{sp}}{\kappa_{bf}} + [3(1 - \phi_{in}) - 1]\right.$$

$$+\left[\left((3\phi_{in}-1)\frac{\kappa_{sp}}{\kappa_{bf}}+(3(1-\phi_{in})-1)\right)^2+8\frac{\kappa_{sp}}{\kappa_{bf}}\right]^{1/2}\Bigg] \tag{19}$$

The aggregate volume fraction is the volume fraction per largest aggregate packing fraction given by

$$\phi_a=\phi\left(\frac{r_a}{r_{sp}}\right)^{3-D},$$

ϕ is nanoparticle volume fraction, ϕ_m is the maximum volume fraction of nanoparticles, $[\chi]$ is Einstein coefficient, D is the fractal index, r_a & r_{sp} are radii of aggregates and nanoparticles, respectively. The Nusselt number and local skin friction coefficient are the physical quantities of concern for the transport phenomenon defined as

$$Nu_x=\frac{-x\kappa_{nf}}{\kappa_{bf}(T_w-T_\infty)}\frac{\partial T}{\partial z},\quad Nu_y=\frac{-y\kappa_{nf}}{\kappa_{bf}(T_w-T_\infty)}\frac{\partial T}{\partial z}$$
$$C_f=\frac{\mu_{nf}}{\rho_{bf}a^2x^2}\frac{\partial u}{\partial z}\qquad C_g=\frac{\mu_{nf}}{\rho_{bf}a^2y^2}\frac{\partial v}{\partial z}. \tag{20}$$

Next is to use Reynolds numbers $\sqrt{Re_y}=\frac{a^{1/2}y}{\vartheta_{bf}^{1/2}}$, $\sqrt{Re_x}=\frac{a^{1/2}x}{\vartheta_{bf}^{1/2}}$ and the similarity variables in Eq. (12) to derive the unitless physical quantities as

$$f''(0)=\frac{C_{fx}\sqrt{Re_x}}{A_2},\ g''(0)=\frac{C_{gy}\sqrt{Re_y}}{cA_2},\quad \frac{Nu_x}{A_4\sqrt{Re_x}}=-\theta'(0) \tag{21}$$

2.2 METHOD OF SOLUTION AND RELIABILITY OF RESULTS

In order to establish the reliability of the obtained solutions, shooting technique procedure of quadratic interpolation (Muller's method) embedded with fourth-order Runge-Kutta Gill integration scheme (`shrkg`) and inbuilt `bvp4c` Matlab package were used to numerically solve Eq. (11) - Eq. (14) for a limiting case $A_2/A_1=A_4/A_3=1$, $c=[0.3,0.4,0.5]$, $P_r=6$, and $f_w=0.3$; see Animasaun [25] for the algorithm of the shooting technique procedure of quadratic interpolation (Muller's method) embedded with the fourth-order Runge-Kutta Gill integration scheme. Based on the results presented in Table (2), it is worth concluding that both methods produced the same results; hence the numerical integration is correct, and the results are reliable.

TABLE 2. Validation and reliability of results for a limiting case $A_2/A_1 = A_4/A_3 = 1$, $c = [0.3, 0.4, 0.5]$, $P_r = 6$, and $f_w = 0.3$

c	$f''(0)$ $shrkg$	$f''(0)$ $bvp4c$	$g''(0)$ $shrkg$	$g''(0)$ $bvp4c$	$-\theta'(0)$ $shrkg$	$-\theta'(0)$ $bvp4c$
0.3	−1.3632	−1.3632	−0.3205	−0.3205	4.6015	4.6015
0.4	−1.3776	−1.3776	−0.4452	−0.4452	4.6522	4.6522
0.5	−1.3955	−1.3955	−0.5836	−0.5836	4.7150	4.7150

3. ANALYSIS AND DISCUSSION OF RESULTS

The data presented in Table (2) was used to simulate the aforementioned transport phenomenon. Because of the changes in viscosity and thermal conductivity, Figure (2) and Figure (3) show the effect of suction (f_w) on the fluid flow of aluminum oxide nanoparticle aggregation and copper(II)oxide nanoparticle aggregation. Suction moves the flow in an upward direction and a forward direction, decreasing the flow. It is noted that under an increased suction parameter value, copper(II)oxide nanoparticle aggregation experiences a more significant decline than aluminum oxide nanoparticle aggregation. Since suction is perpendicular to the vertical velocity, the observed decrease in the horizontal flow along the x and y directions reduces pressure. Figure (4) also shows that the effect of suction (f_w) on temperature indicates that aluminum oxide nanoparticle aggregation gradually decreases over copper(II)oxide nanoparticle aggregation as the suction parameter values increase. Prandtl number is the ratio of momentum diffusivity to thermal diffusivity.

As the Prandtl number rises, as seen in Figure (5), aluminum oxide nanoparticle aggregation decreases faster than Copper(II)oxide nanoparticle aggregation. Figure (6) shows that Copper(II)oxide nanofluid aggregation reduces with a higher stretching ratio c compared to aluminum oxide nanofluid aggregation along with the horizontal velocity in x direction. However, due to a higher stretching ratio c, the copper(II)oxide nanofluid aggregation increases along with the horizontal velocity for the dynamics along the $y-$direction near the wall as shown in Figure (7) compared to aluminum oxide nanofluid aggregation. Physically, a higher magnitude of stretching ratio c leads to a lower stretching rate a. This is the main reason why the horizontal velocity decreases with a higher stretching ratio

in the x direction flow but increases in the $y-$direction flow as observed by Nehad *et al.* [26]. Figure (8) shows that the temperature distribution in aluminum oxide nanoparticle aggregation dynamics decreases with growth in stretching ratio over copper(II)oxide nanoparticle aggregation. In heat transfer, when velocity is increasing, heat energy is transported away from the domain. The observed results in Figure (8) are justifiable because the observed increase in the flow along $y-$direction is not only substantial but also dominates; hence the decrease in the flow along x direction.

Figure (9) and Figure (10) show that the horizontal velocity of both transport phenomena along $x-$direction and $y-$direction is a decreasing property of volume fraction. It is evident based on the information illustrated in Figure (11) that the temperature distribution increases with the volume fraction of nanoparticles. The outcome of the simulation shows that a higher fractal index is capable to causes the velocity of the horizontal velocity along $x-$direction and $y-$direction to increase drastically; see Figure (12) and Figure (13). The analysis of the results suggests that increasing fractal index is capable to cause a decrease in the temperature distribution; see Figure (14). It is worth remarking that the horizontal velocity along $x-$direction and $y-$direction increase due to higher maximum volume fraction of nanoparticles; Figure (15) and Figure (16). Figure (17) depicts that the temperature distribution decreases negligible due to an increase in the maximum volume fraction of nanoparticles. When the radii of aggregates and nanoparticles increase, it is very clear that the temperature distribution increases but the velocity is a decreasing property; see Figure (18), Figure (19), and Figure (20). For brevity, this is shown in Table (3) and Table (4). The local skin friction coefficients $f''(0)$ and $g''(0)$ decrease with increasing values of dual stretching and suction parameters comparatively for copper(II)oxide nanoparticle aggregation and aluminum oxide nanoparticle aggregation. While the reverse is the case for the Nusselt number for the two cases. Using the slope linear regression through the data point suggested by Shah *et al.* [27], Animasaun *et al.* [28], Wakif *et al.* [29], the data presented in Table (3) and Table (4) were further explored. As suction and dual stretching increase, it is worth remarking that the rate of decrease in the local skin friction coefficients proportional to the friction is maximum in the transport phenomenon of water conveying alumina nanoparticles. However, for a significantly large

heat transfer rate as suction and dual stretching increase, dynamics of water conveying cupric nanoparticles should be considered.

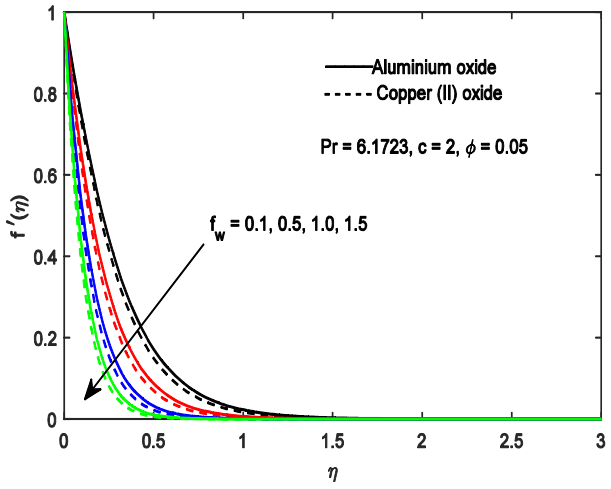

FIGURE 2. Variation in the velocity along $x-$direction with suction

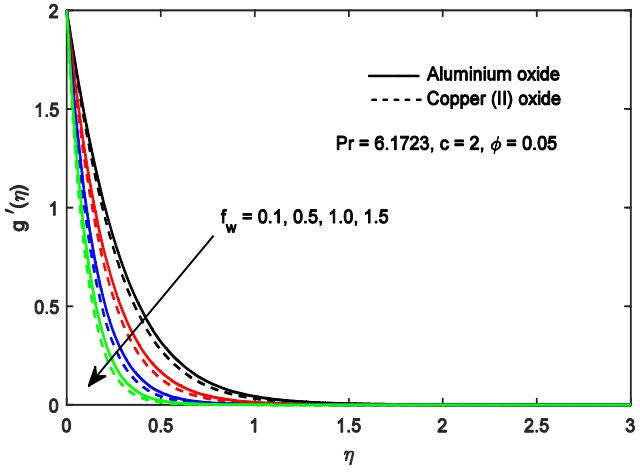

FIGURE 3. Variation in the velocity along $y-$direction with suction

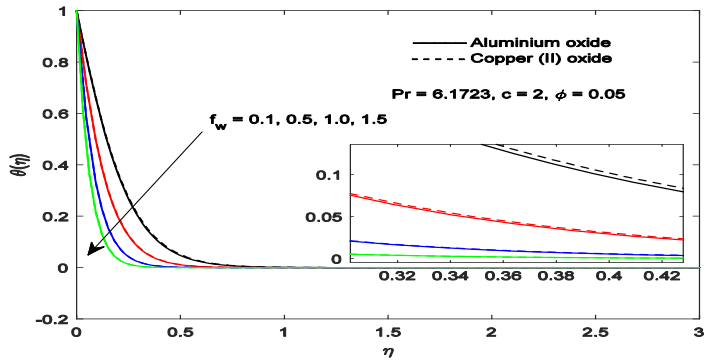

FIGURE 4. Variation in the temperature distribution with suction

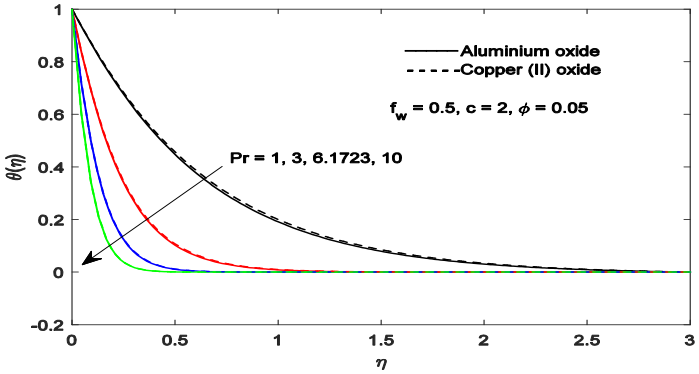

FIGURE 5. Variation in the temperature distribution with Prandtl number

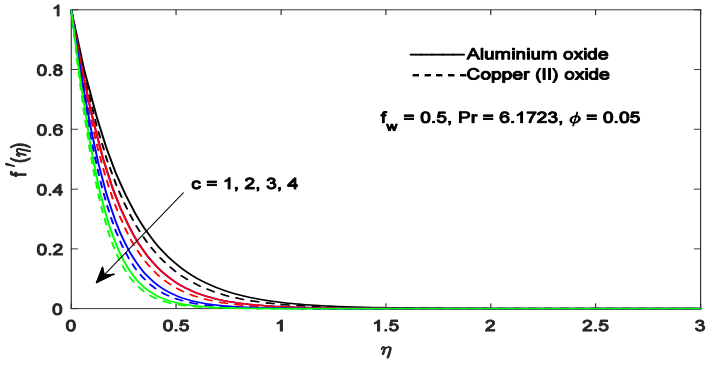

FIGURE 6. Variation in the velocity along $x-$direction with dual stretching

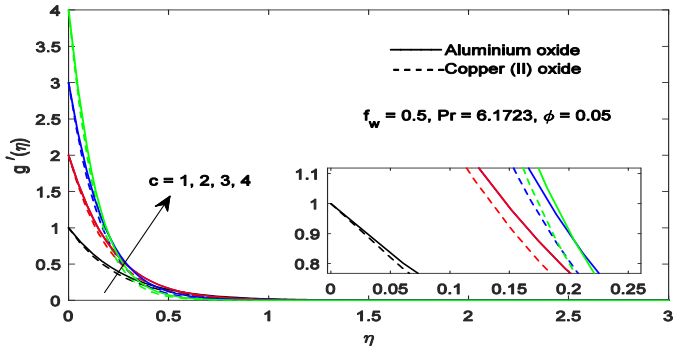

FIGURE 7. Variation in the velocity along y-direction with dual stretching

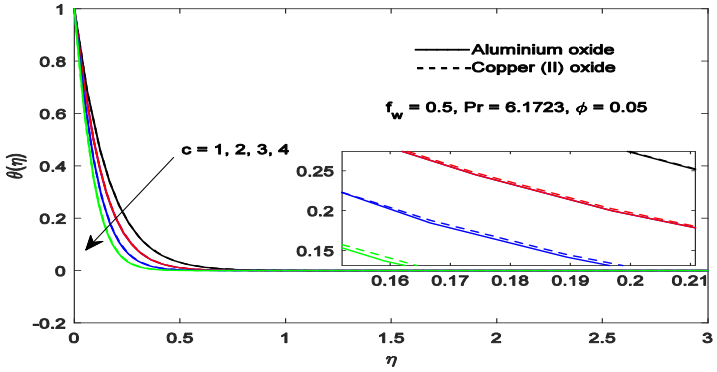

FIGURE 8. Variation in the temperature distribution with dual stretching

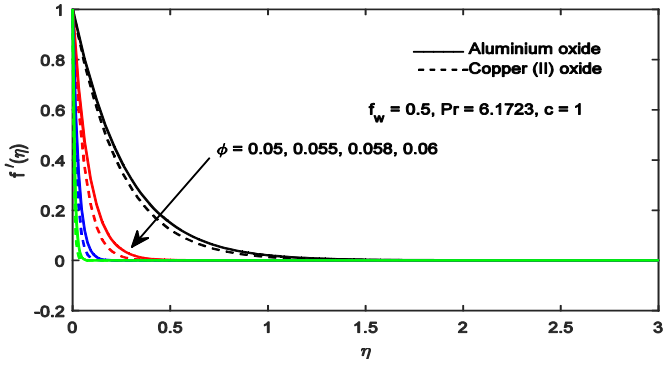

FIGURE 9. Variation in the velocity along $x-$direction with Nanoparticle volume fraction

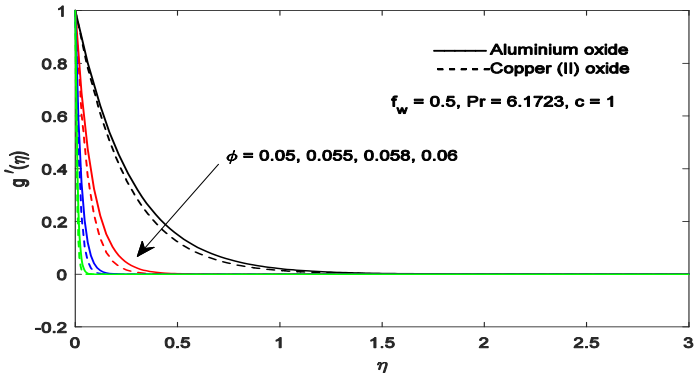

FIGURE 10. Variation in the velocity along $y-$direction with nanoparticle volume fraction

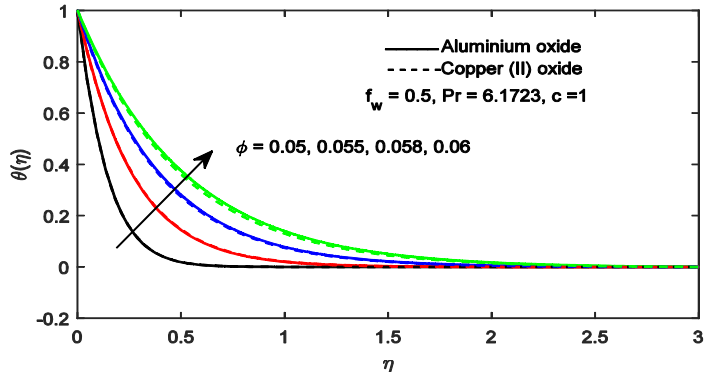

FIGURE 11. ariation in the temperature distribution with nanoparticle volume fraction

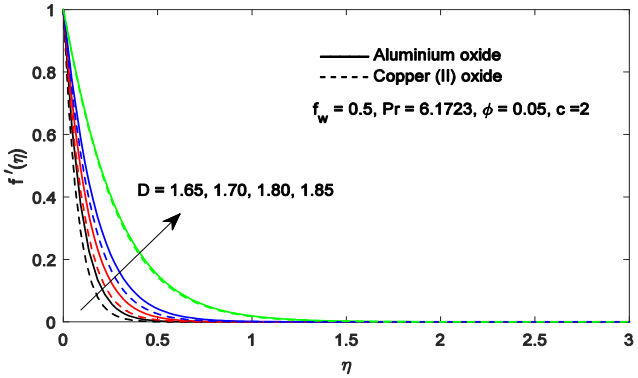

FIGURE 12. Variation in the velocity along $x-$direction with fractal index

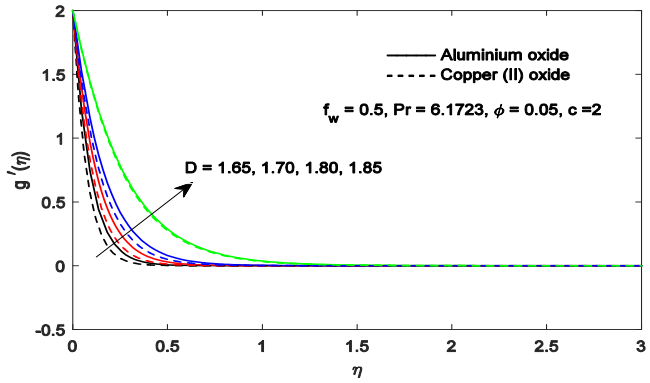

FIGURE 13. Variation in the velocity along $y-$direction with fractal index

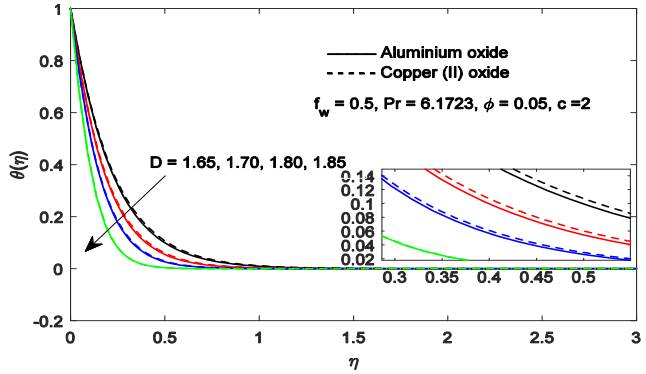

FIGURE 14. Variation in the temperature distribution with fractal index

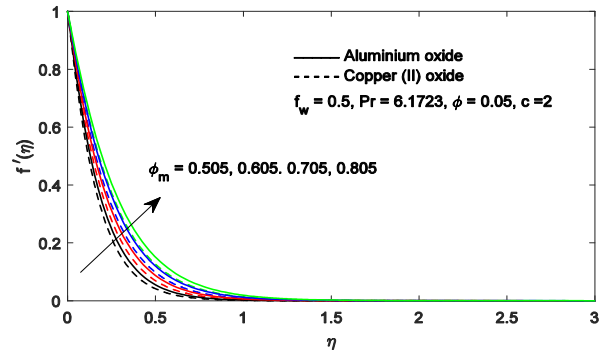

FIGURE 15. Variation in the velocity along $x-$direction with maximum volume fraction of nanoparticles

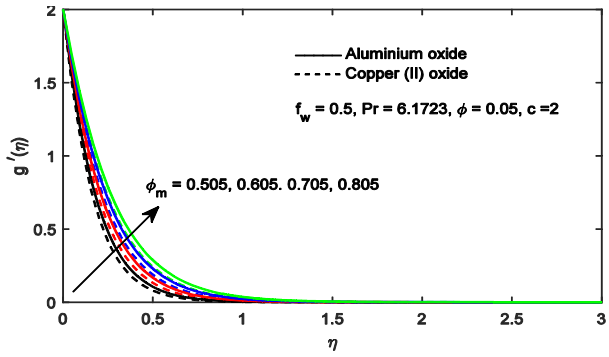

FIGURE 16. Variation in the velocity along y-direction with maximum volume fraction of nanoparticles

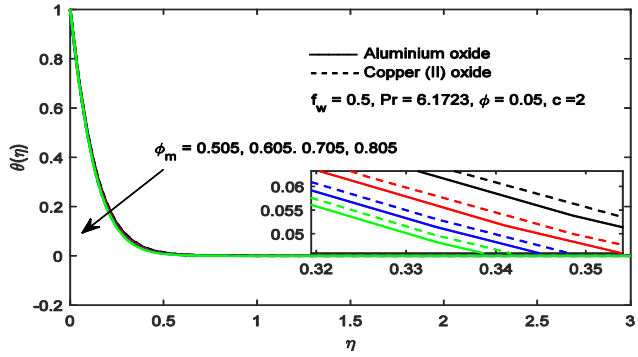

FIGURE 17. Variation in the temperature distribution with maximum volume fraction of nanoparticles

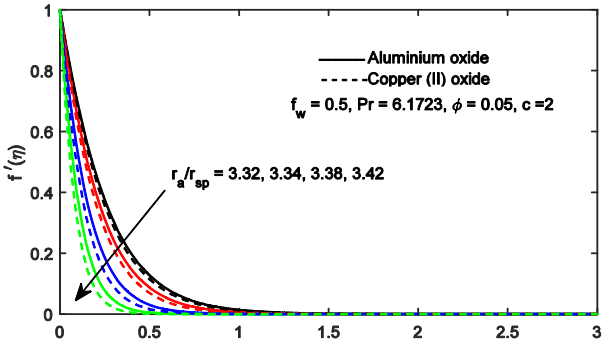

FIGURE 18. Variation in the velocity along $x-$direction with radii of aggregates and nanoparticles

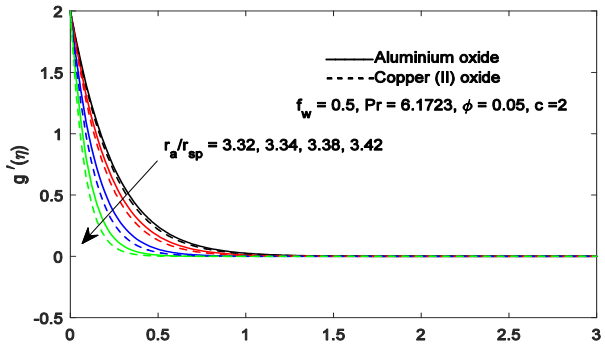

FIGURE 19. Variation in the velocity along $y-$direction with radii of aggregates and nanoparticle

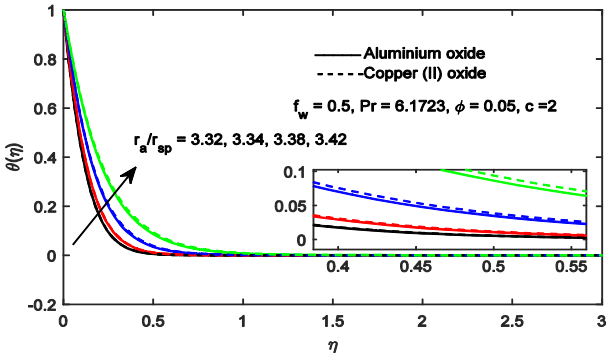

FIGURE 20. Variation in the temperature distribution with radii of aggregates and nanoparticles

5. CONCLUDING REMARKS

In this report, the significance of suction and dual stretching on the dynamics of water-based alumina nanoparticle aggregation and water-based cupric nanoparticle aggregation had been investigated using the modified Maxwell-Bruggeman model. Based on the analysis of results, it is worth concluding that

(1) in the case of nanoparticle aggregation, the higher fractal index is capable to enhance the velocity of both nanofluids because the aggregate volume fraction is strongly dependent on the fractal index. However, such an occurrence declines temperature distribution owing to the associated decrease in viscosity.

TABLE 3. Effect of dual stretching on the local skin friction coefficients and Nusselt number of both nanofluids flow for $\phi = 0.05$, $f_w = 0.5$, $P_r = 6.1723$.

c	Al_2O_3			CuO		
	$f''(0)$	$g''(0)$	$-\theta'(0)$	$f''(0)$	$g''(0)$	$-\theta'(0)$
0.5	−2.94278992	−1.41841639	4.52194116	−3.20529136	−1.55107531	4.52957279
2	−3.64663853	−7.53761619	5.48234278	−3.92839959	−8.09440435	5.46920942
3	−4.30168670	−13.39249059	6.31302080	−4.75731520	−14.83457919	6.62725317
4	−4.98748025	−20.59714962	7.11975616	−5.71130388	−23.81236196	7.99016505
S_{lp}	−0.584372194	−5.43619259	0.74478109	−0.713438454	−6.28381792	0.984246568

TABLE 4. Effect of suction on the local skin friction coefficients and Nusselt number of both nanofluids flow for $\phi = 0.05$, $c = 2$, and $P_r = 6.1723$.

f_w	Al_2O_3			CuO		
	$f''(0)$	$g''(0)$	$-\theta'(0)$	$f''(0)$	$g''(0)$	$-\theta'(0)$
1	−2.95788343	−6.19471406	4.10890501	−5.25119495	−10.61735979	7.06909703
2	−4.64699660	−9.49150851	6.85223448	−8.60657868	−17.26965923	11.27835636
3	−6.48555536	−13.11866072	9.77158013	−13.79529819	−27.65321631	19.51337008
4	−8.39379593	−16.90379140	12.76731022	−16.64722680	−33.32767603	22.13886467
S_{lp}	−1.814629626	−3.575438423	2.889456128	−3.937681506	−7.85145058	5.344431664

(2) the velocity functions are decreasing properties of radii of aggregates and nanoparticles, volume fraction, and suction. In such a case, the observed decreasing property in the velocity is associated with the enhancement in the viscosity of both nanofluids when radii of aggregates and nanoparticles, volume fraction, and suction grow.
(3) the temperature distribution across the transport phenomena is a decreasing property of (a) Prandtl number, (b) dual stretching, (c) fractal index, and (d) maximum volume fraction of nanoparticles. The reverse is the case of volume fraction as it boosts the temperature distribution.
(4) increasing suction and dual stretching is a yardstick to decline local skin friction coefficients proportional to heat transfer rate but cause Nusselt number proportional to the heat transfer rate. The rate of decrease in the local skin friction coefficients proportional to the friction is maximum in the transport phenomenon of water conveying alumina nanoparticles.
(5) as suction and dual stretching increase, a significantly large heat transfer rate is achievable during the dynamics of water conveying cupric nanoparticles should be considered
(6) at different levels of suction at the wall, the velocity in both horizontal directions and the temperature of water conveying alumina nanoparticle aggregation is higher than that of copper-water nanoparticle aggregation because it is less dense but possesses higher heat capacity and thermal conductivity. This is also true at different magnitudes of dual stretching except that the difference between both motions is insignificant.

ACKNOWLEDGEMENTS

The authors are thankful to the Editor-in-Chief of the Journal of the Nigerian Mathematical Society and the honorable Reviewers for their constructive suggestions.

References

[1] W. Zhang, Nanoparticle aggregation: Principles and modeling. Nanomaterial, 19 - 43, 2014.
[2] H. M. Ali, Hybrid nanofluids for convection heat transfer, Academic press, oxford OX5 1GB, United Kingdom, 2020.
[3] S. A. Angayarkanni, J. Philip, Effect of nanoparticles aggregation on thermal and electrical conductivities of nanofluids, Journal of Nanofluids 3(1), 17 - 25, 2014.

[4] A. A. Keller, H. Wang, D. Zhou, H. S. Lenihan, G. Cherr, B. J. Cardinale, M. Robert, Z. Ji, Stability and aggregation of metal oxide nanoparticles in natural aqueous matrices, Environmental Science & Technology 44(6), 1962 - 1967, 2010.

[5] P. Babakhani, The impact of nanoparticle aggregation on their size exclusion during transport in porous media: One- and three-dimensional modelling investigations, Scientific Reports, 9(1) 2019.

[6] Y. He, Y. Jin, H. Chen, Y. Ding, D. Cang, H. Lu, Heat transfer and flow behaviour of aqueous suspensions of TiO2 nanoparticles (nanofluids) flowing upward through a vertical pipe, International journal of heat and mass transfer 50 (11-12), 2272 - 2281, 2007.

[7] J. Mackolil, B. Mahanthesh, Inclined magnetic field and nanoparticle aggregation effects on thermal Marangoni convection in nanoliquid: A sensitivity analysis, Chinese Journal of Physics 69, 24-37, 2021.

[8] R. Prasher, Effect of aggregation on thermal conduction in colloidal nanofluids. Appl. Physi. Lett. 89, 1431119, 2006

[9] A. Katherine, D. Guzman, M. P. Finnegan, J. F. Banfield, Influence of surface potential on aggregation and transport of Titania nanoparticles, Environmental Science Technology, AMS, 40(24) 7688-7693, 2006.

[10] C. Kleinstreuer, Y. Feng, Experimental and theoretical studies of nanofluid thermal conductivity enhancement: a review, Nanoscale Research Letters 6, 229, 2011.

[11] Gaganpreet, S. Srivastava, Effect of aggregation on thermal conductivity and viscosity of nanofluids, Applied Nanoscience 2, 325 - 331, 2012.

[12] R. Ellahi, M. Hassan, A. Zeeshan, Aggregation effects on water base Al2O3-nanofluid over permeable wedge in mixed convection, Asia-Pacific Journal of Chemical Engineering 11(2), 179 - 186, 2016.

[13] J. Peddiesona, A. J. Chamkha, Modeling of Nanofluid Aggregation, Current Nanomaterials 1, 117 - 123, 2016.

[14] M. Marin, M. M. Maskeen, A. Zeeshan, O. U. Mehmood, M. Hassan, Hydromagnetic transport of iron nanoparticle aggregates suspended in water. Indian journal of physics 93, 53 - 59, 2019.

[15] J. Chen, C. Y. Zhao, B. X. Wang, Effect of nanoparticle aggregation on the thermal radiation properties of nanofluids: An experimental and theoretical study, International Journal of heat and mass transfer 154, 119690, 2020.

[16] I. L. Animasaun, O. K. Koriko, K. S. Adegbie, H. A. Babatunde, R. O. Ibraheem, N. Sandeep, B. Mahanthesh, Comparative analysis between 36 nm and 47 nm alumina-water nanofluid flows in the presence of Hall effect. J. Therm. Anal. Calorim. 135(2), 873 - 886, 2018.

[17] A. F. Nanja, W. W. Focke, N. Musee, Aggregation and dissolution of aluminium oxide and copper oxide nanoparticles in natural aqueous matrixes, SN Applied Sciences 2, 1164, 2020

[18] N. A. Aladdin, N. Bachok, I. Pop, Cu-Al2O3/water hybrid nanofluid flow over a permeable moving surface in presence of hydromagnetic and suction effects, Alexandria Engineering Journal 59(2), 657 - 666, 2020.

[19] P. A. Devi, S. S. Devi, Numerical investigation of hydromagnetic hybrid Cu-Al2O3/water nanofluid flow over a permeable stretching sheet with suction, Int. J. Nonlinear Sci. Numerical Simulation 17(5), 249 - 257, 2016.
[20] A. Nadeem, S. Nadeem, A. Saleem, Computational analysis of water-based Cu-Al2O3/H20 over a vertical wedge, Advances in Mechanical Engineering 12(11), 1 - 10, 2020.
[21] L. Prandtl, Uber Flussigkeitsbewegung bei sehr kleiner Reibung translated to motion of fluids with very little viscosity. Internationalen Mathematiker-Kongresses in Heidelberg, 8 - 18, 1904.
[22] B. C. Sakiadis, Boundary layer behavior on continuous solid surfaces: the boundary layer on a continuous flat surface. American Institute of Chemical Engineers 7, 221 - 225, 1961.
[23] M. Sheikholeslami, T. Hayat, A. Alsaedi, MHD free convection of Al_2O_3-water nanofluid considering thermal radiation: A numerical study, International Journal of Heat and Mass Transfer 96, 513 - 524, 2016.
[24] S. A. Mohammadein, K. Raslan, E. M. Abedel-Aal, KKL-model of MHD CuO-nanofluid flow over a stagnation point stretching sheet with nonlinear thermal radiation and suction/injection, Results in Physics 10, 194 - 199, 2018.
[25] I. L. Animasaun, Dynamics of unsteady MHD convective flow with thermophoresis of particles and variable thermo-physical properties past a vertical surface moving through binary mixture, Open Journal of Fluid Dynamics 5, 106 - 120, 2015.
[26] A. S. Nehad, I. L. Animasaun, W. Abderrahim, O. K. Koriko, R. Sivaraj, K. S. Adegbie, Z. Abdelmalek, H. Vaidyaa, A. F. Ijirimoye, K.V. Prasad, Significance of suction and dual stretching on the dynamics of various hybrid nanofluids: Comparative analysis between type I and type II models, Physica Scripta 95, 095205, 2020.
[27] N.A. Shah, I.L. Animasaun, R.O. Ibraheem, H.A. Babatunde, N. Sandeep, I. Pop, Scrutinization of the effects of Grashof number on the flow of different fluids driven by convection over various surfaces, Journal of Molecular Liquids 249, 980 - 990, 2018.
[28] I. L. Animasaun, R. O. Ibraheem, B. Mahanthesh, H.A. Babatunde, A meta-analysis on the effects of haphazard motion of tiny/nano-sized particles on the dynamics and other physical properties of some fluids. Chinese Journal of Physics 60, 676 - 687, 2019.
[29] A. Wakif, I. L. Animasaun, P. V. Satya Narayana, G. Sarojamma, Meta-analysis on thermo-migration of tiny/nano-sized particles in the motion of various fluids. Chinese Journal of Physics 68, 293 - 307, 2020.

DEPARTMENT OF MATHEMATICS, NIGERIA MARITIME UNIVERSITY, OKERENKOKO, DELTA NIGERIA.
E-mail address: kanasogwa@gmail.com

DEPARTMENT OF MATHEMATICAL SCIENCES, FEDERAL UNIVERSITY OF TECHNOLOGY AKURE, ONDO STATE, NIGERIA.
E-mail addresses: ilanimasaun@futa.edu.ng & anizakph2007@gmail.com